Applied Radiation and Isotopes 197 (2023) 110826

Contents lists available at ScienceDirect

Applied Radiation and Isotopes

journal homepage: www.elsevier.com/locate/apradiso

# Comparative study on gamma-ray detectors for in-situ ocean radiation monitoring system

Seungeun Lee [a], Junsung Park [b], Jae Sung Lee [a,c], Hee Seo [b], Guen Bae Ko [c], Jung-Min Seo [d], Soo Mee Kim [d,*]

[a] *Department of Biomedical Sciences, Seoul National University, 103 Daehak-Ro, Jongno-Gu, Seoul, 03080, Republic of Korea*
[b] *Department of Quantum System Engineering, Jeonbuk National University, 567 Baekje-Daero, Deokjin-Gu, Jeonju-Si, Jeollabuk-Do, 54896, Republic of Korea*
[c] *Brightonix Imaging Inc., 25 Yeonmujang 5ga-Gil, Seongdong-Gu, Seoul, 04782, Republic of Korea*
[d] *Maritime ICT & Mobility Research Department, Korea Institute of Ocean Science and Technology, 385 Haeyang-Ro, Yeongdo-Gu, Busan, 49111, Republic of Korea*

ARTICLE INFO

*Keywords:*
GAGG-SiPM detector
NaI(Tl)-PMT detector
In-situ ocean radiation monitoring
Spectrometers
MCNP simulation
Homeland security

ABSTRACT

Large-sized crystals and state-of-the-art photosensors are desirable to cope with low environmental radioactivity (e.g., 1–2 Bq•m$^{-3}$ $^{137}$Cs in surface seawater) for homeland security purposes. We compared the performances of two different gamma-ray detector assemblies, GAGG crystal + silicon photomultiplier (SiPM) and NaI(Tl) crystal + photomultiplier tube, for our mobile in-situ ocean radiation monitoring system. We performed energy calibration, followed by water tank experiments with varying the depth of a $^{137}$Cs point source. Experimental energy spectra were compared with MCNP-simulated spectra with identical setup and the consistency was validated. We finally assessed the detection efficiency and minimum detectable activity (MDA) of the detectors. Both GAGG and NaI detectors exhibited favorable energy resolutions (7.98 ± 0.13% and 7.01 ± 0.58% at 662 keV, respectively) and MDAs (33.1 ± 0.0645 and 13.5 ± 0.0327 Bq•m$^{-3}$ for 24-h $^{137}$Cs measurement, respectively). Matching the geometry of the GAGG crystal with that of the NaI crystal, the GAGG detector outperformed the NaI detector. The results demonstrated that the GAGG detector is potentially advantageous over the NaI detector in detection efficiency and compactness.

## 1. Introduction

The vast ocean has been pioneered for various uses, including coolant tanks for nuclear power plants (NPPs), space for floating marine NPP (Buongiorno et al., 2017; Lee et al., 2015; Yaoli Zhang et al., 2018), and storage of radioactive wastes (Calmet and Bewers, 1991). The ocean is therefore exposed to the risk of radioactive contamination owing to various possibilities such as the meltdown of NPP, disapproved disposal of high-level radioactive wastes ($10^4$ -$10^6$ TBq•m$^{-3}$) (IAEA, 2009), and nuclear submarine accidents (IAEA, 2015; Mian et al., 2019). The spread of damage in the ocean can be minimized with expeditious awareness of radioactive contamination and prompt response to potential further damage-causing events. Long-term investigation of ocean radioactivity is also necessary to follow up on the worldwide dynamics of the radioactive release and address its future effects on the ecosystem and human health. Traditionally, ocean radioactivity was monitored by measuring the radioactivity of sampled seawater in the laboratory. However, sample-based analysis is incapable of immediately controlling radioactive dispersion and requires expensive transportation and processing of the seawater samples. To overcome these limitations, in-situ maritime monitoring is necessary. One widely-used approach is installation of radiation detectors on static buoys (Alexakis and Tsabaris, 2021; Byun et al., 2020; Tsabaris et al., 2021; Wedekind et al., 1999). For deep-sea measurement, a detector tethered to the ship via a long cable is transported to the seafloor (Jones, 2001; Osvath and Povinec, 2001; Thornton et al., 2013).

Enabling the monitoring systems to move freely can significantly increase the efficiency of radiation monitoring in the desired regions that are not covered by a limited number of static detectors. Previously, we developed the first prototype of an in-situ and real-time radiation monitoring system loaded in a remotely controllable unmanned surface vehicle (USV) (Lee et al., 2020) which would contribute to homeland security. The gamma-ray detector was based on a single small CsI(Tl) crystal (10 × 10 × 20 mm$^3$) coupled with a silicon PIN diode. The main limitation of the first prototype was its low detection efficiency and poor minimum detectable activity (MDA) to detect the daily fluctuations in

* Corresponding author.
*E-mail address:* smeekim@kiost.ac.kr (S.M. Kim).

https://doi.org/10.1016/j.apradiso.2023.110826
Received 12 December 2022; Received in revised form 7 March 2023; Accepted 14 April 2023
Available online 15 April 2023

the ocean activity level. To overcome this limitation, a larger crystal with high detection efficiency and superior energy resolution should be used. Photosensors with a low noise level are also preferred to enhance the signal-to-noise ratio of the readout.

Gadolinium aluminum gallium garnet ($Gd_3Al_2Ga_3O_{12}$; GAGG) is a promising scintillator material for radiation detectors in various applications such as radiation protection and medical imaging (Choghadi et al., 2021; Kobayashi et al., 2017; Kochurikhin et al., 2020; Murata et al., 2021; Shikaze and Shimazoe, 2021; Stewart et al., 2016; Takyu et al., 2021; Yajima et al., 2022). GAGG features high effective atomic number and density (Table 1); it is appropriate for energy spectroscopy because of its superior energy resolution by high light yield (Table 1), and also because of the absence of intrinsic radioactivity unlike lutetium- or lanthanum-based scintillators. Non-hygroscopicity of GAGG helps avoid packing problems in the system construction, especially in the humid conditions of the ocean. GAGG is under active research by improving its performance (Kang et al., 2022) and reducing the cost with the hdevelopment of mass production technologies (Kochurikhin et al., 2020) or implementation of ceramic processes (Park et al., 2017).

Silicon photomultiplier (SiPM) was selected to convert the scintillations from GAGG to electric signals. A single SiPM channel is a highly granulated array of microcells connected in parallel and is operated in Geiger-Muller mode (Gundacker and Heering, 2020; Piemonte et al., 2016). Multi-channel SiPMs can effectively cover large areas of the scintillators. Bias voltage for operating the typical SiPM is relatively low (<100 V) compared to traditional photomultiplier tubes (PMTs, hundreds of V). The energy resolution can be further improved by using SiPMs whose wavelength response of photon detection efficiency moderately matches the peak wavelength of GAGG (40–50% at 520 nm depending on SiPM manufacturer and model). The compact size of the SiPM is appropriate for a system with limited space, enabling field radiation monitoring and imaging by being installed on portable devices (Cates et al., 2022; Jeong and Hammig, 2020; Jiang et al., 2016; Morishita et al., 2020; Shimazoe et al., 2020). Combining GAGG and SiPM has successfully imaged ground radioactivity distribution when incorporated with aerial vehicles (Jiang et al., 2016; Shimazoe et al., 2020). Owing to these advantages, a GAGG crystal coupled with SiPMs was considered an appropriate detector for ocean radiation monitoring applications.

A combination of a thallium-doped sodium iodide (NaI(Tl)) scintillation crystal and a PMT is one of the most widely-used radiation detectors (Casanovas et al., 2013; Cinelli et al., 2016) and it was employed for ocean radiation monitoring as well (Povinec et al., 1996; Tsabaris et al., 2018; Zhang et al., 2020). A NaI(Tl) crystal features high energy resolution (6.7% at 662 keV; Table 1) and low cost. The main advantages of a PMT over SiPM are temperature-independent signal gain, low dark count, and simplicity in signal readout (Ko and Lee, 2015; Lee et al., 2018). As NaI(Tl) and PMT assemblies with a wide variety of designs are available in the market, this type was also considered a good candidate for our application.

The aim of this study is to evaluate the performance of a new promising detector (GAGG + SiPM; so-called GAGG detector in this paper) for the practical operation of our in-situ ocean radiation monitoring system with exploring its advantage over a widely used detector (NaI + PMT; so-called NaI detector). To our best knowledge, MDA of GAGG-based detectors has not been studied, and neither GAGG nor SiPM has not been studied with the purpose of ocean radiation monitoring although they showed promising performance in other applications such as positron emission tomography (Choghadi et al., 2021; Kang et al., 2022; Takyu et al., 2021) and ground radioactivity monitoring (Jeong and Hammig, 2020; Jiang et al., 2016; Shikaze and Shimazoe, 2021).

**Table 1**
Physical characteristics of GAGG and NaI(Tl) crystals.

| | GAGG (Stewart et al., 2016) | NaI(Tl) (Moszyński et al., 2002) |
|---|---|---|
| Light yield [$MeV^{-1}$] | 46,000 | 38,000 |
| Intrinsic energy resolution at 662 keV [%] | 5.2 | 6.7 |
| Density [$g \bullet cm^{-3}$] | 6.62 | 3.67 |
| Effective atomic number | 54 | 51 |
| Hygroscopicity | No | Yes |

Fig. 1 shows the overall concept of the in-situ maritime radiation monitoring system. Our ultimate aim is to operate this system for combined long-term and prompt monitoring of the changes in the ocean radioactivity in the region-of-interests. First, we calibrated the channel-to-energy conversion of the detectors and measured their energy resolutions with point source measurements. We additionally obtained the energy spectra of a hot point $^{137}Cs$ inside a water tank with varying depths. As it was impossible to prepare the radionuclide solutions with long half-lives, Monte Carlo simulations were conducted after the validation by comparing the energy spectra with those from the experiments. Finally, we determined the detection efficiency and minimum detectable activity (MDA) for $^{137}Cs$ measurement of the system to investigate the acquisition time interval that provides reliable radioactivity measurement. Further, we discuss the respective features of the detectors in practical operations.

## 2. Materials and methods

### 2.1. Gamma-ray detectors and in-situ monitoring system

#### 2.1.1. GAGG detector

The GAGG detector was composed of a 50 × 50 × 30 $mm^3$ monolithic GAGG crystal (C&A Co., Japan) and multi-channel SiPMs (S13361-3050NE-04; Hamamatsu Photonics K.K., Japan). The GAGG was doped with 1% concentration of cerium (Kamada et al., 2012, 2016; Kochurikhin et al., 2020). The SiPM featured photon detection efficiency of 37% at GAGG peak emission of 520 nm. One 50 × 50 $mm^2$ side of the GAGG crystal was coupled with a 4 × 4 array of SiPMs where each SiPM consisted of 4 × 4 readout channels from 3 × 3 $mm^2$ active areas in a 3.2-mm pitch. No coupling medium was used between the SiPM array and the crystal. A custom 3D-printed gantry made of 3-mm ABS polymer was used to fix the coupling and to shield it from external light. On the SiPM board, anode signals from the 256 SiPM channels were summed into a single output signal and amplified for energy measurement (BASP-10002; Brightonix Imaging Inc., Korea) (Song et al., 2019). A bias voltage was collectively applied to the SiPMs by a separate power control board (BASP-10004; Brightonix Imaging Inc., Korea) which was scalable up to eight SiPM boards. The power control board operated by “pControl” software (Brightonix Imaging Inc., Korea) in a remote PC was used to set the SiPM bias voltage (57 V) and monitor the current and temperature of the SiPM board. A multichannel analyzer (MCA; Notice Inc., Korea) digitized the analog SiPM signals at a frequency of 50 MHz and generated energy spectra with a 12-bit resolution.

#### 2.1.2. NaI detector

The tested NaI detector was a complete assembly of a cylindrical 3” × 3” NaI(Tl) crystal and PMT (905–4; ORTEC, USA). The crystal and the PMT were encapsulated by a 0.5-mm-thick aluminum body to shield them from light and moisture. A bias voltage of 830 V was consistently supplied to the PMT in this study. The signals from PMT were fed into electronics (digiBASE; ORTEC, USA) that integrate bias voltage supply, signal shaping, and MCA.

#### 2.1.3. USV

The system components including the radiation detector, communication equipment, and battery were carried by the USV on the sea surface (Lee et al., 2020). The USV frame was approximately 170-cm long and was made of 1-cm thick carbon fiber reinforced polymer (FRP). The crystal side of each detector was attached to the bottom center inside the USV. During the USV operation, the detector

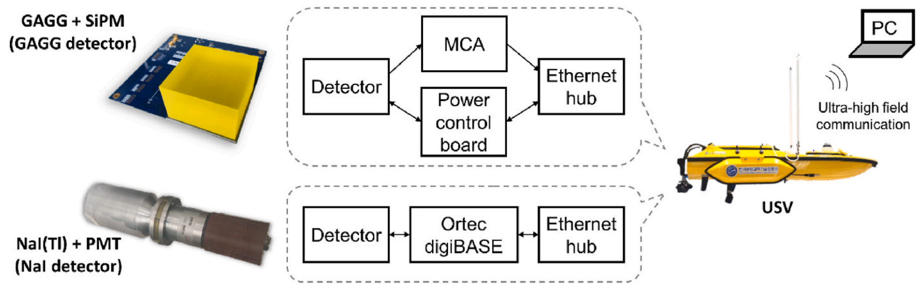


**Fig. 1.** Schematic of the system configuration. GAGG and NaI detectors were individually installed inside the USV.

components were connected to an ethernet hub, which featured ultra-high frequency communication with an up-to-8-km-distant PC, for receiving the SiPM or PMT voltage control signal and transmitting the current and temperature data (Fig. 1). Movements of the USV were automated using "MissionPlanner" software (CHC Navigation Ltd., China).

### 2.2. Experiments

#### 2.2.1. Point radioactive source measurement for energy calibration

For both GAGG and NaI detectors, we acquired $^{137}$Cs, $^{22}$Na, and $^{133}$Ba point source spectra to assess the channel numbers at 662 keV, 511 keV + 1274 keV, and 31 keV + 81 keV +356 keV peaks, respectively. The activities of $^{137}$Cs, $^{22}$Na, and $^{133}$Ba sources were 3.46 mBq, 2.83 mBq, and 3.62 mBq, respectively, and the acquisitions were conducted until the photopeaks were clearly observed. Here, the electronics (MCA and power control board of the GAGG detector, digiBASE of the NaI detector) were directly connected to the PC without remote communication. The setup was placed inside a temperature control box to set and maintain the SiPM temperature at 20 °C and to shield it from the light. We left the setup for about 3 min to make sure that a thermal equilibrium was made. In the case of the GAGG detector, we could additionally check the temperature of the SiPM board measured by the temperature sensor on the SiPM board (Song et al., 2019a). Each point source was located at a distance of 13 cm from the top outer surface of the detector assembly. We measured the energy resolution in percentage full-width at half-maximum (%FWHM) for each energy peak. In the case of the GAGG detector, we additionally obtained $^{137}$Cs spectra at different temperatures to calibrate the gain dependencies on the temperature of the SiPM.

#### 2.2.2. Water tank experiment

The system with each detector was operated inside a 35 × 20 × 8 m$^3$ water tank facilitated by the Underwater Test and Evaluation Center of the Korea Institute of Ocean Science and Technology in Pohang, Korea. We first obtained a background spectrum with all communication equipment turned on to measure the background count rate (shown in the first column of Fig. 6) and subtracted it from further measurements. The USV statically floated on the water with a 3.7 kBq $^{137}$Cs point source tied with a rope, at varying depths of 15, 25, 40, 65, 90, and 115 cm below the USV bottom (Fig. 2). For each depth, we obtained the energy spectrum for 10 min by recording the temperature of the SiPM board for the post-correction of the temperature effect.

#### 2.2.3. Validation of the simulation

The experimental setup described in Sections 2.2.1 and 2.2.2 were reproduced using MCNP6.2 code for the validation (Werner et al., 2018). Several components that can affect the simulation such as the carbon FRP body, lithium-ion batteries, and mechanical supports as well as the detection system were appropriately modeled to simulate the water tank experiments. However, some components were simplified or ignored. For example, we have replaced electronic components for signal processing with uniform simple boxes and ignored cables, which have a relatively small impact on simulation results. Only photons were transported (i.e., mode p) under KERMA approximation for improved computational efficiency. The default cut-off energy of 1 keV in the MCNP code was applied for the photons. The number of primary particles in the simulation (i.e., history) was selected to meet the requirement of relative error within 5%, which was in the range of 1e8 to 1e9 for our simulation cases. To the ideal energy spectrum (i.e., perfect energy resolution) obtained from the simulation, we added a Gaussian random blurring of which the %FWHM was inversely proportional to the square root of energy, based on the energy resolution values measured in Section 2.2.1. The acquired energy spectra in the experiment and simulation were compared.

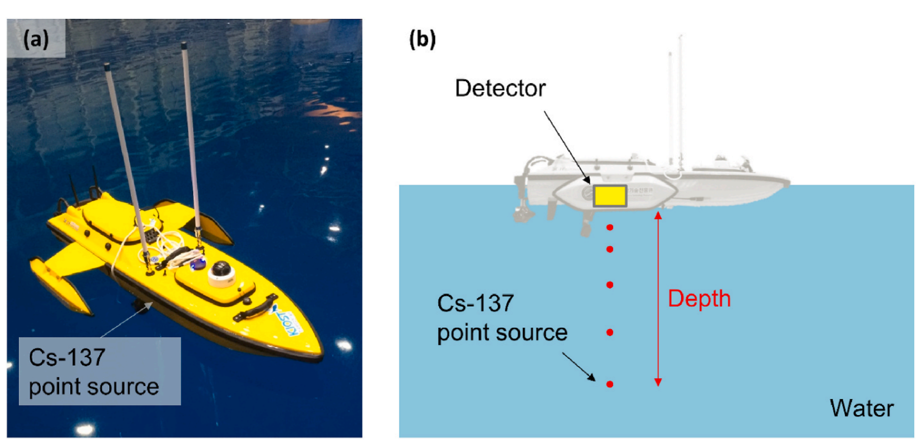


**Fig. 2.** Water tank experiment to investigate the source detectability over depth. (a) Photograph of the USV measuring energy spectra of the tied $^{137}$Cs point source. (b) Schematic of the source depth setup.

### 2.3. Detection efficiency and MDA

Once the reliability was validated in Section 2.2.3, the MCNP method was used to assess the detection efficiency of the system for several gamma-ray energies (Bagatelas et al., 2009; Zhang et al., 2015; Yingying Zhang et al., 2018). The detection efficiency ($\varepsilon$) was defined as the count rate relative to the underwater activity concentration. Here, we define activity concentration as activity per unit volume of water (Bq•m$^{-3}$). Using simulation, we can assess the detection efficiency by dividing the count rate (cps) by the known activity concentration of a detectable volume (Bq•m$^{-3}$).

To emulate the real monitoring of ocean surface activity, the system was assumed to be placed on the measurement spot and measure a uniform source in a cylindrical volume under the detector, covering a 2-$\pi$ bottom view of the detector (Wallace, 2013). The center of the crystal was placed on the center axis of the source cylinder. To determine the detectable volume size, we measured the detection efficiency of each detector for a 1 MBq•m$^{-3}$ uniformly distributed isotropic 1460 keV gamma source within a water volume gradually increasing the radius and height of the cylinder (Fig. 3). First, we fixed the height of the cylinder as 10 cm and increased the radius (Fig. 3(a)). Once we observed that the detection efficiencies of both detectors start to saturate from the radius of 100 cm, we fixed the radius as 100 cm and then increased the height of the cylinder. The height was determined to be 100 cm (Fig. 3 (b)). Once the detectable cylindrical volume was determined, we calculated the detection efficiencies with the isotropic source in the same cylinder with different gamma-ray energies from 90 to 1460 keV.

For both detectors, we measured the background spectrum with all the system components turned on for 24 h and recorded every hour data. A 1460-keV peak of environmental $^{40}$K in the background spectrum was used as a reference to compare the simulation and measurement results. We used $^{40}$K activity concentration of seawater referring to the literature (Yingying Zhang et al., 2018) which was 1.112 Bq•m$^{-3}$ ± 10%. The uncertainties of the detection efficiencies were estimated using the Poisson standard deviation of the photopeak counts ($\sigma = \sqrt{count}$) for both measurements and simulations.

Based on the detection efficiency determined from the simulations, the Currie formula was used to calculate the MDA for several energy points with a confidence level of 95% as follows (Currie, 2002):

$$\mathrm{MDA} = \frac{2.71 + 4.65\sqrt{N_B}}{\varepsilon P_\gamma t}\ (\mathrm{Bq} \bullet \mathrm{m}^{-3}),$$

where $P_\gamma$ and $t$ denote the probability of the target gamma emission per decay and acquisition time, respectively. $P_\gamma$ in this study was set as 94.6% which corresponds to the 662-keV gamma emission probability of Cs-137 decay. $N_B$ at the energy point $E$ was determined as the background count within the energy window of $E \pm$ %FWHM, where % FWHM denotes the fitted value of the results from Section 2.2.1.

## 3. Results

### 3.1. Energy calibration and resolution

Fig. 4 shows the channel-to-energy conversions and their fittings with $R^2$ of 0.9994 and 0.9990 for the GAGG and NaI detectors, respectively. The energy resolutions of the GAGG and NaI detectors were 7.98 ± 0.13% and 7.01 ± 0.58% in FWHM at 662 keV, respectively (the uncertainties denote the half widths of 95% confidence intervals in Gaussian fitting). The measured spectra are shown in Fig. 5. The energy spectra obtained from the measurements and the corresponding simulation were compared, as shown in Fig. 5. The spectra were normalized with the peak counts at 511, 662, and 81 keV for $^{22}$Na, $^{137}$Cs, and $^{133}$Ba, respectively. The overall simulated spectra reflected the distribution of the photopeaks and Compton regions of the measured spectra except for the $^{133}$Ba spectrum measured by the NaI detector. This discrepancy shows the poor energy linearity of the NaI detector in the low-energy region below 100 keV.

### 3.2. Detectability over depth

As the point source was placed distantly from the USV, the count rate of the 662-keV peak significantly decreased because of high attenuation by water and small cross-sectional area of the point source facing the detector (Fig. 6). For both detectors, the count rates within the 662-keV peaks were barely observed when the source depth was larger than 65 cm. High counts in the low-energy region indicate that a substantial proportion of gamma-rays underwent Compton scatterings before reaching the detector. The water tank experiments were well reproduced with the simulations, implying that the simulation is accurately modeling the gamma-ray interactions within the water before reaching the detector.

The results also imply that the mobility of the detection system is critical for the scenario of the presence of a hot source volume within water. To overcome high attenuation underwater and short detectable distance, the detection system should freely approach the source within 50 cm to address the situation.

### 3.3. Detection efficiency and MDA

The detection efficiency for the energies assessed by simulation is shown in Fig. 7. The curve reflected a balance between low photoelectric interaction probability of high energy gamma-rays and high attenuation of low energy gamma-rays before reaching the detector. The measured 1460-keV detection efficiencies of GAGG and NaI were (3.09 ± 0.326) × 10$^{-5}$ and (6.74 ± 0.700) × 10$^{-5}$ cps•(Bq•m$^{-3}$)$^{-1}$, respectively. The simulated efficiencies for 1460-keV detection of the GAGG and NaI detectors were (3.32 ± 0.0009) × 10$^{-5}$ and (6.50 ± 0.0013) × 10$^{-5}$ cps•(Bq•m$^{-3}$)$^{-1}$, therefore the relative differences of measurement to simulation were −7.0% and 3.6% for the GAGG and NaI detectors, respectively. In the case of 662-keV from $^{137}$Cs, the simulated efficiencies of the GAGG and NaI detectors were (4.10 ± 0.0011) × 10$^{-5}$

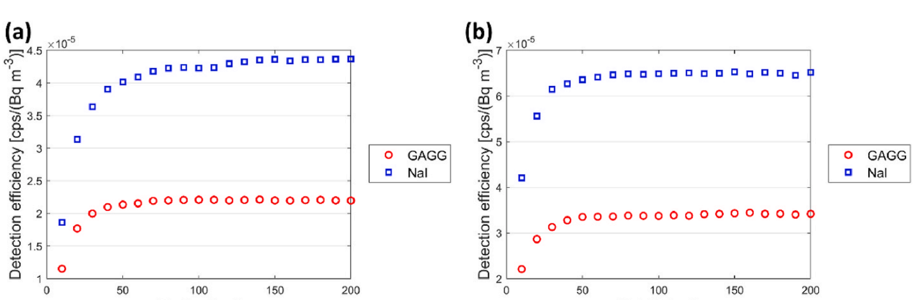


**Fig. 3.** Determination of the detectable volume of the water cylinder with a uniformly distributed 1460-keV isotropic gamma-ray source using simulation. The detection efficiencies of GAGG and NaI detectors were assessed by (a) increasing the radius with a fixed height (10 cm) and (b) increasing the height with a fixed radius (100 cm). The detectable volume was finally determined as a cylinder with both radius and height of 100 cm where the detection efficiencies of both detectors started to saturate.

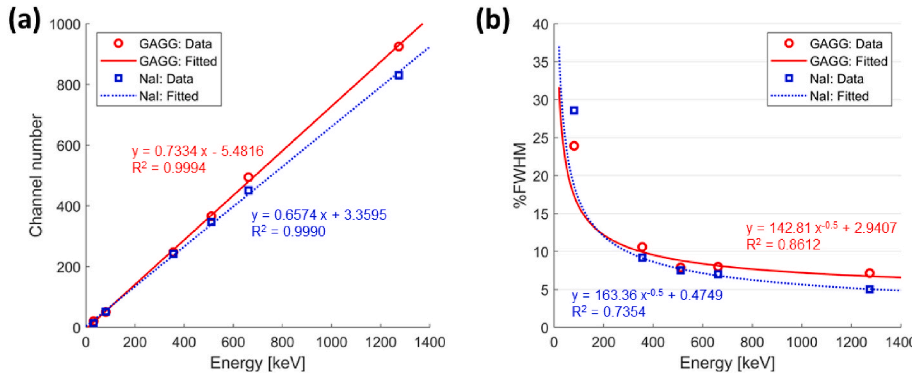


**Fig. 4.** Results of the point source measurements for energy calibration. (a) Channel versus the corresponding energy with linear fitting. (b) Energy resolution in % FWHM versus energy with inverse square root fitting.

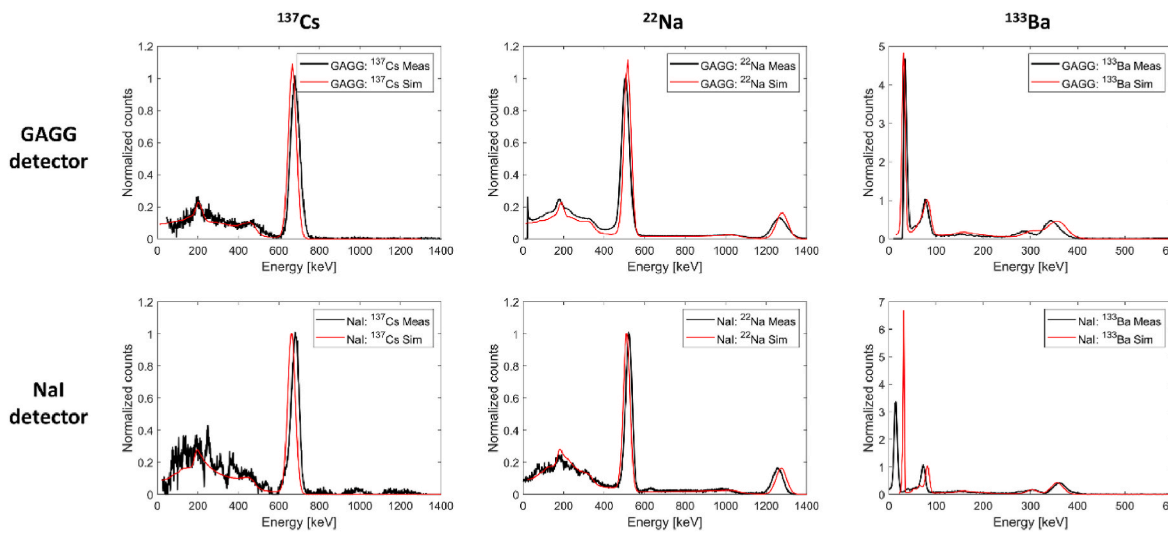


**Fig. 5.** $^{137}$Cs, $^{22}$Na, and $^{133}$Ba spectra obtained from the measurements and simulations of GAGG and NaI detectors.

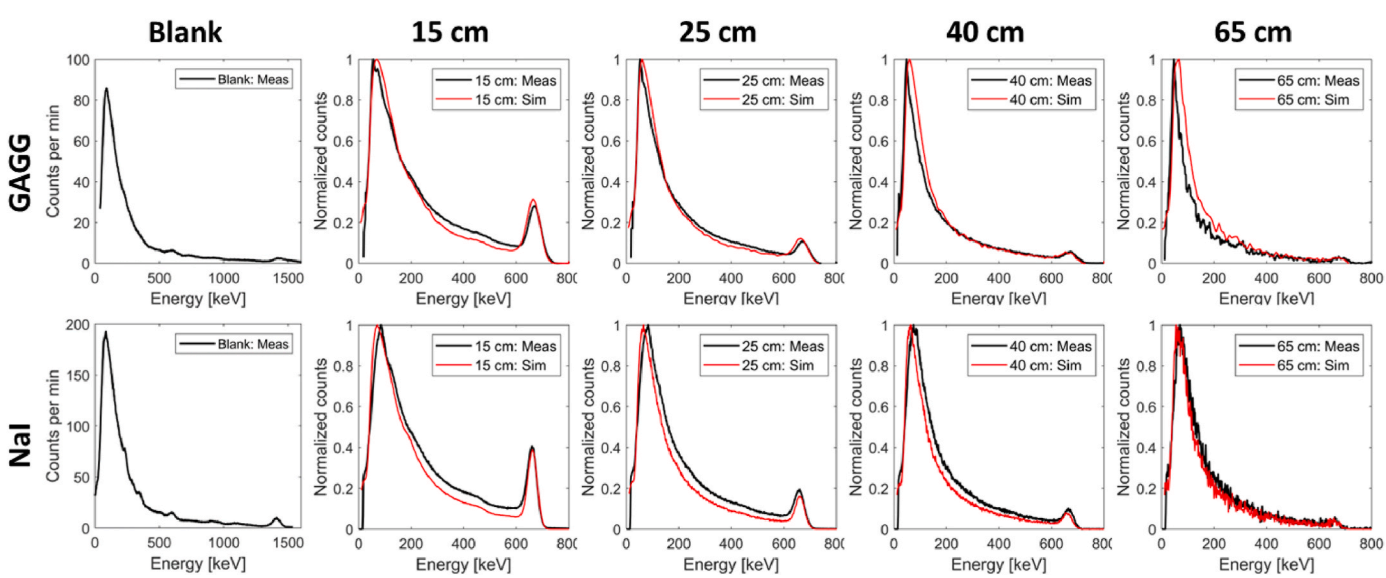


**Fig. 6.** Spectra of background and underwater $^{137}$Cs at different depths obtained from the measurements and simulations of the NaI and GAGG detectors.

and (7.60 ± 0.0015) × $10^{-5}$ cps•(Bq•m$^{-3}$)$^{-1}$, respectively. The NaI detector exhibited approximately 80% higher detection efficiency than the GAGG detector due to the larger volume. Relative to the GAGG detector, the NaI detector achieved low MDA owing to high detection efficiency (Fig. 8). The 24-h MDAs for $^{137}$Cs measurement of the GAGG and NaI detectors were 33.1 ± 0.0645 and 13.5 ± 0.0327 Bq•m$^{-3}$,

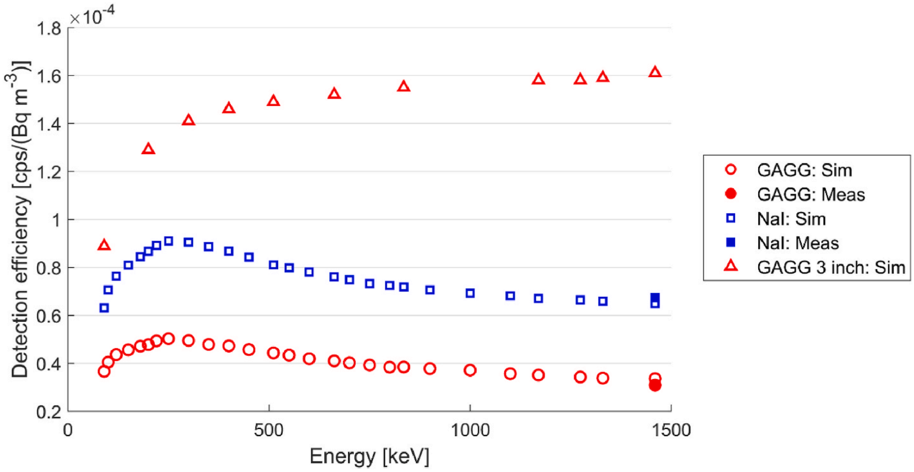


**Fig. 7.** Detection efficiencies of the GAGG and NaI detectors at various energy points. The filled points indicate the in-field measurements of 1460-keV gamma-rays of $^{40}$K. The triangular points indicate the simulated values of hypothetical GAGG with an identical volume to that of NaI (3" × 3″).

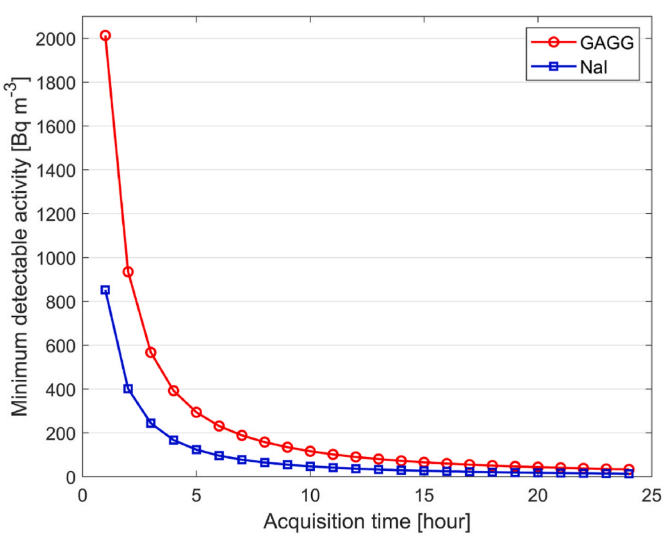


**Fig. 8.** MDAs of GAGG (50 × 50 × 30 mm$^3$) and NaI (3" × 3″) detectors for $^{137}$Cs measurement over the acquisition time assessed with simulation.

respectively.

## 4. Discussion

We tested two different gamma-ray detectors to evaluate their performance and investigate the feasibility of in-situ maritime radiation monitoring. Direct comparison of the performance between the GAGG and NaI detectors was unfair owing to the differences in crystal volumes, photosensors, and readout electronics. An additional simulation was conducted to compare GAGG and NaI with the same crystal size and shape. In the setup described in Section 2.3, the geometry of the GAGG crystal was replaced with a 3" × 3″ cylinder, that is, its volume increased 4.6 times. The peak in detection efficiency curve of the 3" × 3″ GAGG detector appeared at 1.9 MeV which was beyond the energy range of interest in this study. As shown in Fig. 7, the 662-keV detection efficiency of the hypothetical 3" × 3″ GAGG detector was $1.52 \times 10^{-4}$ cps•(Bq•m$^{-3}$)$^{-1}$, which was higher than that of the NaI detector ($7.60 \times 10^{-5}$ cps•(Bq•m$^{-3}$)$^{-1}$) owing to the high density of the GAGG crystal. Consequently, the 24-h MDA for $^{137}$Cs measurement of the 3" × 3" GAGG detector was 8.93 Bq•m$^{-3}$ with assuming a comparable background count rate. The density and effective atomic number of the crystal are key performance factors in detecting photons, particularly for the condition with a very low activity concentration and significant attenuation before reaching the detector.

The optimal volume of GAGG crystal can be determined by assessing detection efficiency as a function of the volume of the detector can be estimated by the simulations. While increasing the volume, the detection efficiency is expected to be saturated at a certain volume where gamma-rays fully deposit their energies. The source with the highest energy of interest (1460 keV in this study) will be simulated to ensure that the detector is able to detect gamma-rays over the entire energies of interest.

From the perspective of in-situ operation, the NaI detector was beneficial because of its simplicity and stability as a commercialized product compared with the prototype GAGG detector. Insensitivity of PMT to temperature is a strong advantage for long-term environmental radiation measurement. Temperature dependency of SiPM can result in photopeak blurring, leading to unreliable measurements of the count rate. High temperature increases the breakdown voltage ($V_{br}$) of SiPM, leading to low overvoltage ($V_{ov}$) and thus low gain when the same bias voltage ($V_{bias}$) is applied ($V_{ov} = V_{bias} - V_{br}$). There are several prospective methodologies to compensate for the SiPM gain dependency on temperature. One simple method is using a look-up-table (LUT) to manually amplify each SiPM signal based on real-time measured temperature (Kwon et al., 2011; Yamamoto et al., 2011). The LUT is generated during the temperature calibration process to correlate the SiPM gain and temperature by saving the amplitude multiplication factor as a function of temperature. Another method is using a temperature compensation circuit that actively controls the $V_{bias}$ using temperature sensor output (Kuznetsov, 2018; Shim et al., 2021). Because the $V_{br}$ and temperature are in a linear relationship as well as temperature sensor output signals, we can add the voltage level of the temperature sensor signal to the voltage supply to keep $V_{ov}$ (or SiPM gain) constant. Still, SiPM is beneficial in scalability owing to its compact size and small dead space, while the voluminous PMT is difficult to install in the small USV.

The new in-situ monitoring system achieved a significant enhancement of MDA compared to the 1st prototype (2500 Bq•m$^{-3}$ for 24-h $^{137}$Cs measurement) owing to the use of large-sized crystals with high density and high atomic number (Lee et al., 2020). Regarding the $^{137}$Cs activity concentration of surface seawater (1–2 Bq•m$^{-3}$) provided by the Korean Nuclear Safety and Security Commission (Korea Institute of Nuclear Safety, 2020), further improvements in MDA are still required to enable the detection of daily fluctuations. The GAGG detector in this study was one single detector unit which will be scaled up with noise enhancements in the follow-up studies. Pursuing to achieve MDA comparable to the normal activity concentration, we could estimate the targeted degree of improvement in MDA, which was larger than 33, considering the current detector unit features the MDA of 33.1 Bq•m$^{-3}$ for 24-h measurement. Once this is achieved, we are planning to operate our system to monitor daily, monthly, and yearly changes in the radioactivity of the seawater in the desired areas. Further improvements in MDA with a few minutes of measurement time required would enable real-time tracking to cope with suspicious radioactive dispersion. For the real operation, a scalability study of the GAGG detector should be performed along with the advancement in electronics regarding stability, noise reduction, and automated temperature compensation (Ko et al., 2016).

## 5. Conclusion

We performed a comparative evaluation of the GAGG + SiPM and NaI(Tl) + PMT gamma-ray detectors for their operations in an in-situ real-time ocean radiation monitoring system. The energy resolutions of the GAGG and NaI detectors were 7.98% and 7.01% at 662 keV, respectively, while the MDAs were 33.1 and 13.5 Bq•m$^{-3}$ for 24-h $^{137}$Cs measurement, respectively. The simulation results showed that we can achieve 8.93 Bq•m$^{-3}$ of the 24-h $^{137}$Cs MDA when we use a GAGG crystal with the same dimension as the NaI used in this study. The high detection efficiency of GAGG and the compactness of SiPM can enable the GAGG detector to outperform the NaI detector when it is scaled up and integrated with advanced electronics in the future.

## CRediT authorship contribution statement

**Seungeun Lee:** Writing – original draft, Visualization, Validation, Software, Methodology, Investigation, Formal analysis, Data curation, Conceptualization. **Junsung Park:** Visualization, Validation, Software, Methodology, Investigation, Formal analysis, Data curation. **Jae Sung Lee:** Supervision. **Hee Seo:** Supervision. **Guen Bae Ko:** Resources, Methodology. **Jung-Min Seo:** Investigation. **Soo Mee Kim:** Writing – review & editing, Supervision, Project administration, Methodology, Funding acquisition, Conceptualization.

## Declaration of competing interest

The authors declare that they have no known competing financial interests or personal relationships that could have appeared to influence the work reported in this paper.

## Data availability

No data was used for the research described in the article.

## Acknowledgement

This work was supported by the Korea Institute of Ocean Science and Technology (grant number PEA0132); and the Ministry of Oceans and Fisheries, Korea ('Development of Smart Processing Technology for Sea Foods').

## References

Alexakis, S., Tsabaris, C., 2021. Design of an interactive cellular system for the remote operation of Ocean sensors: a pilot study integrating radioactivity sensors. J. Mar. Sci. Eng. 9, 910. https://doi.org/10.3390/JMSE9080910.

Bagatelas, C., Tsabaris, C., Kokkoris, M., Papadopoulos, C.T., Vlastou, R., 2009. Determination of marine gamma activity and study of the minimum detectable activity (MDA) in 4pi geometry based on Monte Carlo simulation. Environ. Monit. Assess. 165, 159–168. https://doi.org/10.1007/S10661-009-0935-4.

Buongiorno, J., Jurewicz, J., Golay, M., Todreas, N., 2017. The offshore floating nuclear plant concept. Nucl. Technol. 194, 1–14. https://doi.org/10.13182/NT15-49.

Byun, J.I., Choi, S.W., Song, M.H., Chang, B.U., Kim, Y.J., Yun, J.Y., 2020. A large buoy-based radioactivity monitoring system for gamma-ray emitters in surface seawater. Appl. Radiat. Isot. 162, 109172 https://doi.org/10.1016/J.APRADISO.2020.109172.

Calmet, D.P., Bewers, J.M., 1991. Radioactive waste and ocean dumping: the role of the IAEA. Mar. Pol. 15, 413–430. https://doi.org/10.1016/0308-597X(91)90051-C.

Casanovas, R., Morant, J.J., Salvadó, M., 2013. Implementation of gamma-ray spectrometry in two real-time water monitors using NaI(Tl) scintillation detectors. Appl. Radiat. Isot. 80, 49–55. https://doi.org/10.1016/j.apradiso.2013.06.003.

Cates, J.W., Steele, J., Balajthy, J., Negut, V., Hausladen, P., Ziock, K., Brubaker, E., 2022. Front-end design for SiPM-based monolithic neutron double scatter imagers. Sensors 22. https://doi.org/10.3390/s22093553.

Choghadi, M.A., Huang, S.C., Shimazoe, K., Takahashi, H., 2021. Evaluation of dual-ended readout GAGG-based DOI-PET detectors with different surface treatments. Med. Phys. 48, 3470–3478. https://doi.org/10.1002/MP.14874.

Cinelli, G., Tositti, L., Mostacci, D., Baré, J., 2016. Calibration with MCNP of NaI detector for the determination of natural radioactivity levels in the field. J. Environ. Radioact. 155–156, 31–37. https://doi.org/10.1016/j.jenvrad.2016.02.009.

Currie, L.A., 2002. Limits for qualitative detection and quantitative determination. Application to radiochemistry. Anal. Chem. 40, 586–593. https://doi.org/10.1021/AC60259A007.

Gundacker, S., Heering, A., 2020. The silicon photomultiplier: fundamentals and applications of a modern solid-state photon detector. Phys. Med. Biol. https://doi.org/10.1088/1361-6560/ab7b2d.

IAEA, 2015. The Fukushima Daiichi Accident. IAEA, Vienna, Austria.

IAEA, 2009. IAEA Safety Standards: Classification of Radioactive Waste for Protecting People and the Environment No. GSG-1 General Safety Guide (Vienna, Austria).

Jeong, M., Hammig, M., 2020. Development of hand-held coded-aperture gamma ray imaging system based on GAGG(Ce) scintillator coupled with SiPM array. Nucl. Eng. Technol. 52, 2572–2580. https://doi.org/10.1016/J.NET.2020.04.009.

Jiang, J., Shimazoe, K., Nakamura, Y., Takahashi, H., Shikaze, Y., Nishizawa, Y., Yoshida, M., Sanada, Y., Torii, T., Yoshino, M., Ito, S., Endo, T., Tsutsumi, K., Kato, S., Sato, H., Usuki, Y., Kurosawa, S., Kamada, K., Yoshikawa, A., 2016. A prototype of aerial radiation monitoring system using an unmanned helicopter mounting a GAGG scintillator Compton camera. J. Nucl. Sci. Technol. 53, 1067–1075. https://doi.org/10.1080/00223131.2015.1089796.

Jones, D.G., 2001. Development and application of marine gamma-ray measurements: a review. J. Environ. Radioact. 53, 313–333. https://doi.org/10.1016/S0265-931X(00)00139-9.

Kamada, K., Shoji, Y., Kochurikhin, V.v., Okumura, S., Yamamoto, S., Nagura, A., Yeom, J.Y., Kurosawa, S., Yokota, Y., Ohashi, Y., Nikl, M., Yoshikawa, A., 2016. Growth and scintillation properties of 3 in. diameter Ce doped Gd3Ga3Al2O12 scintillation single crystal. J. Cryst. Growth 452, 81–84. https://doi.org/10.1016/j.jcrysgro.2016.04.037.

Kamada, K., Yanagida, T., Endo, T., Tsutumi, K., Usuki, Y., Nikl, M., Fujimoto, Y., Fukabori, A., Yoshikawa, A., 2012. 2 inch diameter single crystal growth and scintillation properties of Ce:Gd 3Al 2Ga 3O 12. In: Journal of Crystal Growth, pp. 88–90. https://doi.org/10.1016/j.jcrysgro.2011.11.085.

Kang, H.G., Kim, K.J., Kamada, K., Yoshikawa, A., Yoshida, E., Nishikido, F., Yamaya, T., 2022. Optimization of GFAG crystal surface treatment for SiPM based TOF PET detector. Biomed Phys Eng Express 8. https://doi.org/10.1088/2057-1976/ac56c6.

Ko, G.B., Kim, K.Y., Yoon, H.S., Lee, M.S., Son, J.W., Im, H.J., Lee, J.S., 2016. Evaluation of a silicon photomultiplier PET insert for simultaneous PET and MR imaging. Med. Phys. 43, 72–83. https://doi.org/10.1118/1.4937784.

Ko, G.B., Lee, J.S., 2015. Performance characterization of high quantum efficiency metal package photomultiplier tubes for time-of-flight and high-resolution PET applications. Med. Phys. 42, 510–520. https://doi.org/10.1118/1.4903897.

Kobayashi, T., Yamamoto, S., Yeom, J.Y., Kamada, K., Yoshikawa, A., 2017. Development of high resolution phoswich depth-of-interaction block detectors utilizing Mg co-doped new scintillators. Nucl. Instrum. Methods Phys. Res. 875, 111–118. https://doi.org/10.1016/J.NIMA.2017.08.030.

Kochurikhin, V., Kamada, K., Jin Kim, K., Ivanov, M., Gushchina, L., Shoji, Y., Yoshino, M., Yoshikawa, A., 2020. Czochralski growth of 4-inch diameter Ce:Gd3Al2Ga3O12 single crystals for scintillator applications. J. Cryst. Growth 531. https://doi.org/10.1016/j.jcrysgro.2019.125384.

Korea Institute of Nuclear Safety, 2020. 2020 Marine Environmental Radioactivity Survey.

Kuznetsov, E., 2018. Temperature-compensated silicon photomultiplier. Nucl. Instrum. Methods Phys. Res. 912, 226–230. https://doi.org/10.1016/j.nima.2017.11.060.

Kwon, S. il, Lee, J.S., Yoon, H.S., Ito, M., Ko, G.B., Choi, J.Y., Lee, S.H., Song, I.C., Jeong, J.M., Lee, D.S., Hong, S.J., 2011. Development of small-animal PET prototype using silicon photomultiplier (SiPM): initial results of phantom and animal imaging studies. J. Nucl. Med. 52, 572–579. https://doi.org/10.2967/jnumed.110.079707.

Lee, K.H., Kim, M.G., Lee, J.I., Lee, P.S., 2015. Recent advances in ocean nuclear power plants. Energies 8, 11470–11492. https://doi.org/10.3390/EN81011470.

Lee, S., Lee, J.S., Kim, H.S., Park, J., Baek, S., Song, Y., Seo, J.-M., Kim, S.M., 2020. In-situ remotely controllable ocean radiation monitoring system. J. Instrum. 15, P06027 https://doi.org/10.1088/1748-0221/15/06/P06027.

Lee, S., Lee, M.S., Won, J.Y., Lee, J.S., 2018. Performance of a new accelerating-electrode-equipped fast-time-response PMT coupled with fast LGSO. Phys. Med. Biol. 63 https://doi.org/10.1088/1361-6560/aaad20.

Mian, Z., Ramana, M.V., Nayyar, A.H., 2019. Nuclear submarines in South asia: new risks and dangers. Journal for peace and nuclear disarmament 2, 184–202. https://doi.org/10.1080/25751654.2019.1621425.

Morishita, Y., Ye, Y., Mata, L., Pozzi, S.A., Kearfott, K.J., 2020. Radon measurements with a compact, organic-scintillator-based alpha/beta spectrometer. Radiat. Meas. 137 https://doi.org/10.1016/j.radmeas.2020.106428.

Moszyński, M., Zalipska, J., Balcerzyk, M., Kapusta, M., Mengesha, W., Valentine, J.D., 2002. Intrinsic energy resolution of NaI(Tl). Nucl. Instrum. Methods Phys. Res. 484, 259–269. https://doi.org/10.1016/S0168-9002(01)01964-7.

Murata, I., Kusaka, S., Minami, K., Saraue, N., Tamaki, S., Kato, I., Sato, F., 2021. Design of SPECT for BNCT to measure local boron dose with GAGG scintillator. Appl. Radiat. Isot., 110056 https://doi.org/10.1016/J.APRADISO.2021.110056.

Osvath, I., Povinec, P.P., 2001. Seabed γ-ray spectrometry: applications at IAEA-MEL. J. Environ. Radioact. 53, 335–349. https://doi.org/10.1016/S0265-931X(00)00140-5.

Park, C., Kim, C., Kim, J., Lee, Y., Na, Y., Lee, K., Yeom, J.Y., 2017. Performance comparison between ceramic Ce:GAGG and single crystal Ce:GAGG with digital-SiPM. J. Instrum. 12 https://doi.org/10.1088/1748-0221/12/01/P01002.

Piemonte, C., Acerbi, F., Ferri, A., Gola, A., Paternoster, G., Regazzoni, V., Zappala, G., Zorzi, N., 2016. Performance of NUV-HD silicon photomultiplier Technology. IEEE Trans. Electron. Dev. 63, 1111–1116. https://doi.org/10.1109/TED.2016.2516641.

Povinec, P.P., Osvath, I., Baxter, M.S., 1996. Underwater gamma-spectrometry with HPGe and NaI(Tl) detectors. Appl. Radiat. Isot. 47, 1127–1133. https://doi.org/10.1016/S0969-8043(96)00118-2.

Shikaze, Y., Shimazoe, K., 2021. Improvement of analysis results from the GAGG scintillator Compton camera operated on an unmanned helicopter by selecting stable flight conditions. J. Nucl. Sci. Technol. 59, 44–54. https://doi.org/10.1080/00223131.2021.1948452.

Shim, H.S., Park, H., Lee, J.S., 2021. A temperature-dependent gain compensation technique for positron emission tomography detectors based on a silicon photomultiplier. Phys. Med. Biol. 66 https://doi.org/10.1088/1361-6560/ac2b81.

Shimazoe, K., Yoshino, M., Ohshima, Y., Uenomachi, M., Oogane, K., Orita, T., Takahashi, H., Kamada, K., Yoshikawa, A., Takahashi, M., 2020. Development of simultaneous PET and Compton imaging using GAGG-SiPM based pixel detectors. Nucl. Instrum. Methods Phys. Res. https://doi.org/10.1016/j.nima.2018.10.177.

Song, S.H., Kang, H.G., Han, Y.B., Lee, H.-Y., Jeong, D.-H., Kim, S.M., Hong, S.J., 2019a. Characterization and Validation of Multimodal Annihilation-Gamma/near-Infrared/visible Laparoscopic System, 096008. https://doi.org/10.1117/1.JBO.24.9.096008, 10.1117/1.JBO.24.9.096008 24.

Stewart, A.G., Seitz, B., O'neill, K., Wall, L., Jackson, J.C., 2016. Energy resolution of Ce:GAGG and Pr:LuAG scintillators coupled to 3 mm × 3 mm silicon photomultipliers. IEEE Trans. Nucl. Sci. 63, 2496–2501. https://doi.org/10.1109/TNS.2016.2574773.

Takyu, S., Nishikido, F., Yoshida, E., Nitta, M., Kamada, K., Yoshikawa, A., Yamaya, T., 2021. GAGG–MPPC detector with optimized light guide thickness for combined Compton-PET applications. Nucl. Instrum. Methods Phys. Res. 990, 164998 https://doi.org/10.1016/J.NIMA.2020.164998.

Thornton, B., Ohnishi, S., Ura, T., Odano, N., Fujita, T., 2013. Continuous measurement of radionuclide distribution off Fukushima using a towed sea-bed gamma ray spectrometer. Deep Sea Res. Oceanogr. Res. Pap. 79, 10–19. https://doi.org/10.1016/J.DSR.2013.05.001.

Tsabaris, C., Androulakaki, E.G., Alexakis, S., Patiris, D.L., 2018. An in-situ gamma-ray spectrometer for the deep ocean. Appl. Radiat. Isot. 142, 120–127. https://doi.org/10.1016/j.apradiso.2018.08.024.

Tsabaris, C., Androulakaki, E.G., Ballas, D., Alexakis, S., Perivoliotis, L., Iona, A., 2021. Radioactivity monitoring at north aegean sea integrating in-situ sensor in an ocean observing platform. J. Mar. Sci. Eng. 9, 77. https://doi.org/10.3390/JMSE9010077.

Wallace, J.D., 2013. Monte Carlo modelling of large scale NORM sources using MCNP. J. Environ. Radioact. 126, 55–60. https://doi.org/10.1016/J.JENVRAD.2013.06.009.

Wedekind, C., Schilling, G., Grüttmüller, M., Becker, K., 1999. Gamma-radiation monitoring network at sea. Appl. Radiat. Isot. 50, 733–741. https://doi.org/10.1016/S0969-8043(98)00062-1.

Werner, C.J., Bull, J.S., Solomon, C.J., Brown, F.B., McKinney, G.W., Rising, M.E., Dixon, D.A., Martz, R.L., Hughes, H.G., Cox, L.J., Zukaitis, A.J., Armstrong, J.C., Forster, R.A., Casswell, L., 2018. MCNP Version 6.2 Release Notes. https://doi.org/10.2172/1419730.

Yajima, K., Kim, E., Tani, K., Ogawa, M., Igarashi, Y., Kowatari, M., Kurihara, O., 2022. Development of a new hand-held type thyroid monitor using multiple GAGG detectors for young children following a nuclear accident. Radiat. Meas. 150, 106683 https://doi.org/10.1016/J.RADMEAS.2021.106683.

Yamamoto, S., Satomi, J., Watabe, T., Watabe, H., Kanai, Y., Imaizumi, M., Shimosegawa, E., Hatazawa, J., 2011. A temperature-dependent gain control system for improving the stability of Si-PM-based PET systems. Phys. Med. Biol. 56, 2873–2882. https://doi.org/10.1088/0031-9155/56/9/015.

Zhang, Yaoli, Buongiorno, J., Golay, M., Todreas, N., 2018. Safety analysis of a 300-MW (electric) offshore floating nuclear power plant in marine environment. Nucl. Technol. 203, 129–145. https://doi.org/10.1080/00295450.2018.1433935.

Zhang, Y., Wu, B., Liu, D., Lv, H., Feng, X., 2020. Research on minimum detectable activity (MDA) of underwater gamma spectrometer for radioactivity measurement in the marine environment. Appl. Radiat. Isot. 155, 108917 https://doi.org/10.1016/j.apradiso.2019.108917.

Zhang, Yingying, Li, C., Liu, D., Zhang, Ying, Liu, Y., 2015. Monte Carlo simulation of a NaI(Tl) detector for in situ radioactivity measurements in the marine environment. Appl. Radiat. Isot. 98, 44–48. https://doi.org/10.1016/j.apradiso.2015.01.009.

Zhang, Yingying, Wu, B., Liu, D., Zhang, Ying, Cheng, Y., 2018. Development and deployment of an autonomous sensor for the in-situ radioactivity measurement in the marine environment. Appl. Radiat. Isot. 142, 181–186. https://doi.org/10.1016/j.apradiso.2018.10.004.